

Preprint from the Proceedings of the
1981 Symposium on Laser Induced Damage
Boulder, Colorado, November 1981

Two- and Three-Photon Absorption in Semiconductors with
Subsequent Absorption by Photogenerated Carriers

E. W. Van Stryland, M. A. Woodall,
W. E. Williams, and M. J. Soileau

Center for Applied Quantum Electronics
North Texas State University
Denton, Texas 76203

A careful examination of two-photon absorption in CdTe and three-photon absorption in CdS and ZnSe was made by studying the transmission of picosecond pulses at $1.06 \mu\text{m}$ and the photoacoustic signal generated in the sample by the absorption of light. We found that in order to separate the direct nonlinear absorption from the subsequent absorption by the photogenerated carriers, careful analysis of the data over a wide range of irradiance levels was necessary. The nonlinear absorption coefficients for these three materials were determined, as well as an overall excess carrier absorption cross section. In addition, for CdTe we used two different temporal pulsewidths to verify our analysis. The photoacoustic data had a 1 to 1 correspondence with the transmission data indicating that this more sensitive technique should be useful for measuring nonlinear absorption spectra in solids with a variety of less powerful lasers. In addition for samples such as BK7 glass, which showed no nonlinear transmission even when surface damage occurred, the photoacoustic signal showed abrupt large increases when damage occurred. No nonlinear absorption was observed in two types of CVD ZnS prior to damage.

Key Words: nonlinear absorption, photoacoustic, two-photon, three-photon, CdTe, CdS, ZnSe

1. Introduction

Over the past several years there has developed an increased interest in the nonlinear optical properties of semiconductors for use as active elements in integrated optics. Additionally there has been considerable controversy over the initiation process of laser induced damage, multiphoton absorption being a prime candidate for supplying the electrons to start an avalanche [1,2]. As such, the magnitude of 2, 3 and higher order multiphoton absorption processes are of interest. Additionally since selection rules for nonlinear absorption are different than for linear absorption new information on band structure constants are obtained [3,4].

We observed two-photon absorption (2PA) in CdTe by monitoring the transmission and photoacoustic signals using single picosecond $1.06 \mu\text{m}$ laser pulses [5]. A wide range of irradiance levels was used up to the point at which front surface damage occurred. At such high light levels 2PA induced carrier

absorption was the dominant loss mechanism. Even at a relatively low irradiance these excess carriers significantly affected the absorption. We performed these measurements using two different pulse-widths to verify the effects of photogenerated carrier absorption.

Three photon absorption (3PA) in CdS and ZnSe was observed in a similar manner. Again induced carrier absorption was dominant at irradiance levels near those required to produce damage. Nonlinear absorption larger than predicted by 3PA plus induced carrier absorption at high irradiance levels was observed in both samples. No nonlinear absorption was observed in CVD ZnS, either heat treated (Cleartran*) or non-heat treated, or in BK7 glass. A large increase in the photoacoustic signal was observed when the BK7 glass surface damaged. Such a large increase upon damage was not observed in CdTe, CdS, or ZnSe.

2. Theory

The change in light irradiance I of a laser pulse as a function of depth z in a sample which exhibits n -photon absorption is given by

$$\frac{dI}{dz} = -[\alpha I + \beta_n I^n] - \sigma_{ex} N_{ex} I \quad (1)$$

where α is the linear absorption coefficient, and β_n , $n = 2, 3, \dots$ is the multiphoton absorption coefficient [6]. (Lower order multiphoton absorption events are neglected whenever $(n - 1) h\omega < E_{gap}$ the band gap energy). σ_{ex} is the "mean" linear absorption cross section for multiphoton excited electrons and holes with N_{ex} (the number of multiphoton excited carriers) determined by

$$\frac{dN_{ex}}{dt} = \frac{\beta_n I^n}{nh\omega} \quad (2)$$

Recombination and diffusion during the picosecond pulses are neglected. N_{ex} is assumed negligible prior to the laser pulse. Neglecting the excited state absorption ($\sigma_{ex} = 0$) eq. (1) gives

$$I(L, r, t) = \frac{I(0, r, t)(1 - R)^2 e^{-\alpha L}}{\left[1 + \frac{\beta_2}{\alpha} I(0, r, t)(1 - R)(1 - e^{-\alpha L})\right]} \quad \text{for } n = 2 \quad (3)$$

and

$$I(L, r, t) = \frac{I(0, r, t)(1 - R)^2 e^{-\alpha L}}{\left[1 + \frac{\beta_3}{\alpha} I^2(0, r, t)(1 - R)^2(1 - e^{-2\alpha L})\right]^{1/2}} \quad \text{for } n = 3 \quad (4)$$

where R is the surface reflectivity and $I(0, r, t)$ is the irradiance incident on the front surface of the sample. The effects of rear surface reflections, which can be significant for high index

*Cleartran is a trade name for CVS ZnS used by CVC Inc. Woburn, MA, to describe material which has been made "water clear" by a proprietary heat treatment process.

materials, have been neglected. These effects are discussed in Ref. 8. From eqs. 3 and 4 and similar equations for higher order multiphoton absorption processes it is clear that

$$\frac{1}{T^{n-1}} = T^{1-n} = \left[1 + \frac{\beta_n}{\alpha} I^{n-1}(0,r,t)(1-R)^{n-1}(1 - e^{-(n-1)\alpha L})\right] \times \left(\frac{e^{\alpha L}}{(1-R)^2}\right)^{n-1} \quad (5)$$

where T is the transmission through the sample. Thus a plot of T^{1-n} as a function of I^{n-1} yields a straight line whose intercept determines the linear absorption coefficient α , and whose slope determines the nonlinear absorption coefficient β_n . Integrals over the measured Gaussian spatial and temporal profiles give a negative curvature to these lines. We take the incident irradiance to be $I(0,r,t) = I_0 e^{-(r/r_0)^2} e^{-(t/t_0)^2}$ where r_0 and t_0 are the half width at the e^{-1} height for the spatial and temporal profiles respectively. For $n = 2$ and 3 the spatial integral can be performed yielding for two photon absorption

$$\frac{1}{T} = \frac{I_0 \sqrt{\pi} \beta_2 (e^{\alpha L} - 1)}{2 \alpha (1-R)} \int_0^\infty dx \ell_n \left[1 + \frac{\beta_2}{\alpha} I_0 (1-R) (1 - e^{-\alpha L}) e^{-x^2}\right]^{-1} \quad (6)$$

and for three-photon absorption

$$\frac{1}{T^2} = \frac{I_0^2 \pi \beta_3 (e^{2\alpha L} - 1)}{\alpha (1-R)^2} \left\{ \int_0^1 \frac{dx}{x \sqrt{\ell_n \frac{1}{x}}} \ell_n (\sqrt{\delta} x + \sqrt{1 + \delta x^2}) \right\}^{-2} \quad (7)$$

where $\delta = \beta_3 I_0^2 (1-R)^2 (1 - e^{-2\alpha L}) / \alpha$.

The increased sensitivity of the photoacoustic (PA) method over transmission has made PA (opto-acoustic) spectroscopy extremely useful for the determination of small linear absorptivities (down to 10^{-6} cm^{-1}) [9,10,11]. The increased sensitivity is due to the ability of PA spectroscopy to directly measure the absorbed energy, rather than measure a small change in the large transmitted energy. A similar advantage is incurred for nonlinear absorption measurements, however, the total linear absorption then appears as a background [5,7]. In order to observe the nonlinear absorption it must be comparable to the linear absorption. This restriction limits the applicability to low loss samples, which means that pure materials are needed since the photon energy is below the band-gap energy for multiphoton absorbing samples.

Calculating the energy absorbed, E_{abs} , in the sample, which is directly proportional to the PA signal, [10] yields (neglecting rear surface reflections)

$$\frac{E_{\text{abs}}}{E_{\text{inc}}} = 1 - R - \frac{T}{1-R} \quad (8)$$

where E_{inc} is the energy incident on the sample. Equation 8, of course assumes the fluorescence efficiency is small, as was the case for the semiconductors studied. This equality allows us to predict from the transmission measurements what is expected for the PA measurements. For low total absorption, (i.e. $(\alpha + \beta_2 I) L \ll 1$ or $(\alpha + \beta_3 I^2) L \ll 1$ etc.).

$$\frac{1}{\Gamma^{n-1}} = [1 + (n-1)\alpha L + (n-1) \frac{\beta I_0^{n-1}}{n\sqrt{n}} (1-R)^{n-1} L] / (1-R)^{2(n-1)} \quad (9)$$

and

$$\frac{E_{\text{abs}}}{E_{\text{inc}}} = (1-R)L \left[\alpha + \frac{\beta I_0^{n-1}}{n\sqrt{n}} (1-R)^{n-1} \right] \quad (10)$$

showing more explicitly the increased sensitivity of the photoacoustic technique. The term including β_n for the PA method is compared to a term involving α , which can be very small, rather than being compared to unity.

The effects of the absorption of carriers created by nonlinear absorption can be included by numerically solving eqs. 1 and 2 using Gaussian temporal shaped pulses, and then integrating the result over the Gaussian spatial profile. The carrier density is taken to be zero prior to the pulse.

3. Experiment

The laser source used in these experiments was a microprocessor-controlled, mode-locked, Gaussian-mode Nd:YAG laser producing single pulses of up to 10 mJ per pulse at 1.06 μm as shown in figure 1. The pulsedwidth was variable between ~30 and 200 psec (FWHM) by choosing various etalons for the output coupler. The temporal waveform was Gaussian as determined by measuring the second harmonic autocorrelation function, accepting only pulses having a fixed ratio R. R is the ratio of the square of the energy in the fundamental to the energy produced at the second harmonic in a doubling crystal. R is measured by the "t_p monitor" in figure 1. This ratio is directly proportional to the pulsedwidth as was verified by measuring the second order autocorrelation functions for the various etalons [11,6]. Thus the ratio R served as a single shot pulsedwidth monitor. Data was accepted only for pulses having a pulsedwidth within ~15% of the stated value as determined by the ratio R. The spatial profile was determined to be Gaussian by performing pinhole beam scans and by observing the irradiance distribution on a vidicon tube. The energy incident and transmitted was monitored with linear photodiode peak and hold detectors directly calibrated against a GenTec Ed-100 pyroelectric detector which was in turn checked against a thermopile calorimeter. The irradiance was calculated from the energy, beam profile, and pulsedwidth. Absolute irradiances are estimated to be correct within ~35% while relative intensity readings are within ~10%.

Since there is a possibility that the spatial beam profile changes within the sample due to self-focusing or defocusing, we checked the transmitted intensity profiles on a vidicon. Although these were not quantitative measurements, no substantial deviation from the expected broadening due to nonlinear absorption was observed.

The acoustic transducers were 4 mm diameter by 4 mm thick lead zirconate titanate cylinders pressed against the sample surface with a thin coat of vacuum grease [10,12]. The acoustic signal was amplified and fed to a gated detector. The gate was set to sample the peak height of one of the first acoustic spikes caused by bulk absorption. The signal peak voltage has been shown to be directly proportional to the energy absorbed by the sample [10]. The signal produced by light scattered directly

onto the transducer was in several cases small compared to the signals of interest. In some cases the scattered signal could not be ignored and gave the appearance of an anomalously large linear absorption. In other cases such as in ZnSe this signal occurred long enough prior to the bulk absorption signal that it had substantially decayed.

These experiments were specifically designed to allow simultaneous measurement of transmission and optoacoustic signals so that an absolute calibration and direct comparison was possible. Therefore many of the possible advantages of the optoacoustic method were not used.

4. Results

We present nonlinear absorption data at 1.06 μm in CdTe, CdS, and ZnSe. No nonlinear absorption was observed in CVD ZnS either in its heat treated form (Cleartran) or as deposited. No nonlinear transmission was observed in BK7 glass, but when optical damage occurred a very large increase in the photoacoustic signal was observed with only a very slight decrease in transmission.

Figure 2 shows a plot of inverse transmission versus irradiance for relatively low irradiance, 40 psec (FWHM) pulses incident on a 0.30 cm thick polycrystalline CdTe sample. The straight line is a fit using eq. 6 ignoring free carrier absorption. The fit corresponds to $\beta_2 = 35 \text{ cm/GW}$. Bechtel and Smith [6] used a similar technique on single crystal CdTe to obtain a value of 25 cm/GW. We saw no differences in the nonlinear absorption coefficient with slightly thinner single crystal samples. At higher irradiance levels, as shown in figure 3, we see that the data deviates significantly from the solid line which neglects photogenerated carrier absorption. If these excess carriers are included by numerically solving eqs. 1 and 2 and integrating over space and time the dotted line is obtained using a free carrier cross section, σ_{ex} , equal to $2 \times 10^{-16} \text{ cm}^2$ (β_2 remains 35 cm/GW). Figure 4 shows that further deviation from simple two-photon absorption theory (solid line) is seen as the irradiance is increased up to the level where permanent optical damage of the front surface occurs. In fact, the optical absorption from the excess carriers dominates the total absorption near damage. The surface damage is not limited by nonlinear absorption but by surface defects as described in Ref. 14. Figure 4 shows an extension of the dotted line of figure 3. There is only a small deviation from the theory at high irradiance levels. At the highest irradiances less than 10% of the incident light is transmitted. This is seen in figure 5 which is a replot of figure 4 now with transmission as the vertical axis. A comparison of figures 4 and 5, for low transmission T , shows that a plot of T^{-1} is more sensitive to the parameters β_2 and σ_{ex} than a similar plot of T . The reasons for the observed deviations are unclear but the theory is certainly oversimplified. The fact that such a good fit is obtained up to 2 GW/cm^2 where the surface damages and where the carrier density is calculated in this model to be 10^{19} 1/cm^3 is really quite remarkable.

The fits obtained are unfortunately not unique. The method used was to fit the very lowest irradiance ignoring excess carriers to obtain β_2 , and then to include photogenerated carrier absorption to fit higher irradiance data. For example, if we use the data of figure 3, ignore carriers and fit this data to obtain β_2 , we find $\beta_2 = 50 \text{ cm/GW}$. As shown in figure 6 this fit appears to be quite good over this limited irradiance range. If, however, we now try to add in the effects of photogenerated carriers to explain the higher irradiance data we cannot obtain nearly as good an overall fit. This observation may explain some of the disagreement in reported values for two-photon absorption coefficients. If a limited range of irradiance is used and excess carrier absorption is not carefully included, different coefficients can be obtained using different pulsewidth lasers. Indeed one might also "observe" a pulsewidth dependence of the nonlinear absorption coefficient as has been reported,

[13] and explained using the above argument [14]. In order to verify that the deviation from simple two-photon absorption theory was due primarily to subsequent photogenerated carrier absorption we repeated the experiment using 150 psec (FWHM) pulses. This data is shown in figure 7. Again the solid line is two-photon absorption only. The dotted line includes subsequent excess carrier absorption where again $\beta_2 = 35 \text{ cm/GW}$ and $\sigma_{\text{ex}} = 2 \times 10^{-16} \text{ cm}^2$. A comparison with figure 4 shows that for longer pulses more carriers are created and transmission decreases more rapidly. This is expected since for a given irradiance the energy per pulse is larger. The theory includes these effects (dotted line) and again the fit is quite good. This data confirms the previous analysis and shows that near damage the excess carrier absorption dominates the nonlinear absorption even for picosecond pulses. We estimate that the value of β_2 is within 20% and σ_{ex} is within 50%.

We obtain similar results for the three-photon absorbers CdS and ZnSe. Data for CdS is shown in figure 8 for low I and figure 9 for high I. Data for ZnSe is shown in figure 10. Here for three-photon absorption the inverse of the square of the transmission is plotted versus the square of the irradiance as indicated by eq. 7. The increased scatter for the ZnSe data is because three separate sets of data are shown. The apparatus was disassembled and reassembled between two of the runs. To determine the three-photon absorption coefficient for CdS and ZnSe we used the technique previously discussed for determining two-photon absorption coefficients, namely fitting the low irradiance levels ignoring excess carriers and then including carrier absorption to account for the high irradiance data. For both CdS and ZnSe, however, it was found that the irradiance range over which there was an observable transmission change and a negligible excess carrier contribution to the absorption was extremely limited if not nonexistent. (See Fig. 8) We therefore iterated the procedure using progressively smaller three-photon absorption coefficients and larger free carrier cross sections to obtain a fit over the largest low irradiance range. No combination of these constants could fit the data at the highest irradiance. As was observed with CdTe, the absorption is larger at high irradiance levels than our simple model predicts except that in CdS and ZnSe the deviations are considerably greater. One possible explanation for the deviation is the onset of avalanche breakdown. Additionally very weak second harmonic at $0.53 \mu\text{m}$ was observed in both ZnSe and CdS [13]. The efficiency was much less than a percent and doesn't account for the observed differences. The constants obtained are, for CdS, $\beta_3 = 0.06 \text{ cm}^3/\text{GW}^2$ and $\sigma_{\text{ex}} = 1.5 \times 10^{-17} \text{ cm}^2$. The estimated errors here are much larger (within a factor of 2 for β_3 and for σ_{ex}) because the nonlinearity is higher order and the separation between the pure three-photon absorption and subsequent carrier absorption is not nearly as clean as for CdTe. For ZnSe we obtained $\beta_3 = 0.01 \text{ cm}^3/\text{GW}^2$ and $\sigma_{\text{ex}} = 1 \times 10^{-17} \text{ cm}^2$. Here β_3 and σ_{ex} are known only within an order of magnitude. A pulsewidth dependent study of the nonlinear transmission is in progress to verify this separation.

In the case of CdS a similar transmission experiment on a 0.1 cm thick CdS sample using 7 psec pulses from a mode-locked Nd:glass laser has previously been reported [16]. If the data of Ref. 17 is replotted as in our figure 9 and the irradiance is scaled down by a factor of ~ 2.8 , that data nearly reproduces our data. The difference in sample thicknesses and the shorter pulsewidths used accounts for only part of the irradiance difference. That data was taken using a mode-locked Nd:glass laser and it was not stated whether the laser was operating in a single transverse mode. Glass lasers are notoriously difficult to operate $\text{TEM}_{0,0}$ when mode-locked. Spatial beam inhomogeneities could easily account for a factor of three difference in calculated intensities.

An example of the photoacoustic data is shown in figure 11 for ZnSe. Figure 12 shows what is expected for the photoacoustic data as calculated from the transmission data using eq. 8. The ver-

tical axis of figure 11 was scaled to match that of figure 12. There is a quite good one-to-one correspondence of the data as we reported earlier for two-photon absorption [5]. Data at low irradiances was very noisy both using PA spectroscopy and as calculated from transmission. The deviation at the very highest intensities is probably due to the onset of surface damage. A small pitting of the entrance surface was observed at an incident irradiance of 20 GW/cm^2 ($400 \text{ GW}^2/\text{cm}^4$ in Fig. 11 and 12). If the light were predominantly scattered, the absorption as measured by the transducer could be reduced more than the transmission. The photoacoustic (optoacoustic) technique, thus yields the same information as the transmission experiment when calibrated. It's increased sensitivity when using lower irradiance and higher repetition rate laser systems should prove valuable in the future for the measurement of nonlinear absorption.

5. Conclusion

The results for two-photon absorption in CdTe indicate that great care must be taken in analyzing nonlinear absorption data. Any direct absorption process in a semiconductor will be accompanied by another higher order absorption process; namely photogenerated carrier absorption. We presented a method to separate the contributions of direct nonlinear absorption from the subsequent multiphoton generated carrier absorption. This method necessitates having data over a wide range of irradiances. Taking data using different laser pulsedwidths confirmed the separation to be correct. This separation was shown to be more difficult for higher order nonlinearities by observing three-photon absorption in CdS and ZnSe. In addition, a significant deviation from the simple theory presented at the highest irradiance levels was observed for these materials. A possible explanation is the onset of avalanche breakdown.

All the data indicates that to unambiguously separate the contributions of direct nonlinear absorption from subsequent excess carrier absorption one must use both the shortest possible pulses and the lowest possible irradiance where a signal can still be observed. The photoacoustic technique, used in conjunction with higher repetition rate short pulsed lasers, offers the best possibility of achieving both criteria. In particular we are currently investigating the PA techniques for observing nonlinear absorption of visible light from synchronously pumped mode-locked dye lasers which offer high repetition rate ultrashort pulses.

The authors gratefully acknowledge the support of the Office of Naval Research, the National Science Foundation, The Robert A. Welch Foundation, and the North Texas State Faculty Research Fund.

6. References

- [1] See for example, N. Bloembergen, IEEE, J.Q.E. QE-10, 375 (1974), D. W. Fradin, Laser Focus 41, 45 [1974].
- [2] E. W. Van Stryland, M. J. Soileau, A. L. Smirl, and William E. Williams, Phys. Rev. B1 23, 1 (1981).
- [3] "Two-Photon Spectroscopy" by J. M. Worlock in Laser Handbook V2, 1323-1369, North Holland, 1972.
- [4] C. R. Pidgeon, B. S. Wherrett, A. M. Johnston, J. Dempsey, and A. Miller, Phys. Rev. Letters 42, 1785 (19779).

- [5] E. W. Van Stryland and M. A. Woodall, NBS Special Publication No. 620, 50, 1980.
- [6] J. H. Bechtel and W. L. Smith, Phys. Rev. B13, 3515, 1976.
- [7] M. Bass, E. W. Van Stryland, and A. F. Stewart, Appl. Phys. Lett. 34, 142, 1979.
- [8] Y. A. Pao, "Opto-acoustic Spectroscopy and Detection", Academic Press 1977.
- [9] A. Rosencwaig, "Photoacoustics and Photoacoustic Spectroscopy", Chemical Analysis, Vol. 57, John Wiley, 1980.
- [10] C. K. N. Patel and A. C. Tam, Rev. Mod. Phys. 53, 517 (1981).
- [11] W. H. Glenn and M. J. Brienza, Appl. Phys. Lett. 10, 221 (1967).
- [12] A. Hordvik, and H. Schlossberg, Appl. Opt. 16, 101, 1977.
- [13] M. J. Soileau, William E. Williams, E. W. Van Stryland, and M. A. Woodall, submitted for publication in Applied Optics, 1982.
- [14] A. F. Stewart and M. Bass, Appl. Phys. Lett. 37, 1040 (1980).
- [15] C. R. Pidgeon, A. M. Johnston and J. Dempsey, Proceedings of the 4th International Conference on Physics of Narrow gap Semiconductors, Linz, September 1981.
- [16] A. Penzkofer and W. Falkenstein, Optics. Comm. 16, 247 (1976).

Figure Captions

- Figure 1. Experimental apparatus for monitoring the transmission and the photoacoustic signal in non-linearly absorbing samples.
- Figure 2. Inverse transmission of 40 psec (FWHM) 1.06 μm pulses as a function of incident irradiance on CdTe. The x's are data and the solid line is a theoretical curve for two-photon absorption with $\beta_2 = 35 \text{ cm/GW}$.
- Figure 3. Inverse transmission of 40 psec (FWHM) 1.06 μm pulses as a function of incident irradiance on CdTe. The x's are data and the solid line is a theoretical curve for two-photon absorption with $\beta_2 = 35 \text{ cm/GW}$. The dashed line is a theoretical fit including the effects of excess carrier absorption with $\sigma_{\text{ex}} = 2 \times 10^{-16} \text{ cm}^2$.
- Figure 4. Inverse transmission of 40 psec (FWHM) 1.06 μm pulses as a function of incident irradiance on CdTe. The x's are data and the solid line is a theoretical curve for two-photon absorption with $\beta_2 = 35 \text{ cm/GW}$. The dashed line is a theoretical fit including the effects of excess carrier absorption with $\sigma_{\text{ex}} = 2 \times 10^{-16} \text{ cm}^2$.
- Figure 5. This graph is a replot of figure 4 but with the vertical axis replaced by the transmission.
- Figure 6. This graph shows the same data as in figure 2. The solid line is a fit with $\beta_2 = 50 \text{ cm/GW}$ where excess carriers are ignored.
- Figure 7. Inverse transmission of ~150 psec (FWHM) 1.06 μm pulses as a function of incident irradiance on CdTe. The x's are the data and the solid line is a theoretical curve for two-photon absorption with $\beta_2 = 35 \text{ cm/GW}$. The dashed line is a theoretical fit including the effects of excess carrier absorption with $\sigma_{\text{ex}} = 2 \times 10^{-16} \text{ cm}^2$.
- Figure 8. The inverse of the square of the transmission of 40 psec (FWHM) 1.06 μm pulse as a function of the square of the irradiance on CdS. The x's are data and the solid line is a theoretical curve for a three-photon absorption coefficient of $\beta_3 = 0.06 \text{ cm}^3/\text{GW}^2$. The dashed line is a theoretical fit including the effects of excess carrier absorption with $\sigma_{\text{ex}} = 1.5 \times 10^{-17} \text{ cm}^2$.
- Figure 9. The inverse of the square of the transmission of 40 psec (FWHM) 1.06 μm pulse as a function of the square of the irradiance on CdS. The x's are data and the solid line is a theoretical curve for a three-photon absorption coefficient of $\beta_3 = 0.06 \text{ cm}^3/\text{GW}^2$. The dashed line is a theoretical fit including the effects of excess carrier absorption with $\sigma_{\text{ex}} = 1.5 \times 10^{-17} \text{ cm}^2$.
- Figure 10. The inverse of the square of the transmission of 40 psec (FWHM) 1.06 μm pulses as a function of the square of the irradiance on ZnSe.
- Figure 11. The ratio of the photoacoustic signal in volts to the incident energy in Joules as a function of the square of the incident irradiance of 40 psec (FWHM) 1.06 μm pulses on ZnSe.
- Figure 12. The vertical axis is what is expected for figure 11 as calculated from the transmission data shown in figure 10. See the discussion in the text.

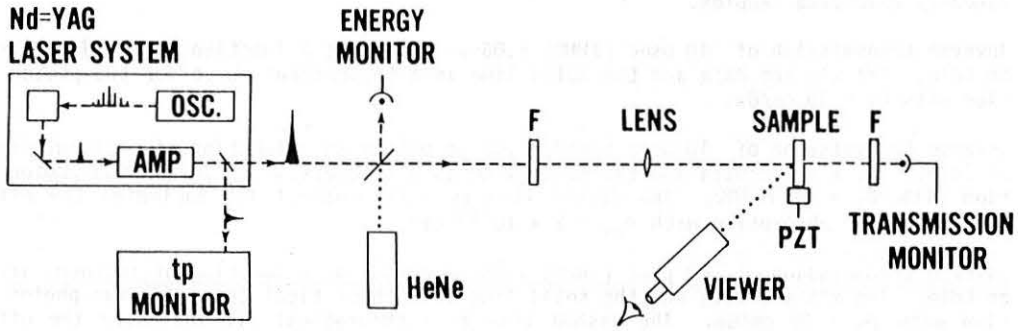


Figure 1

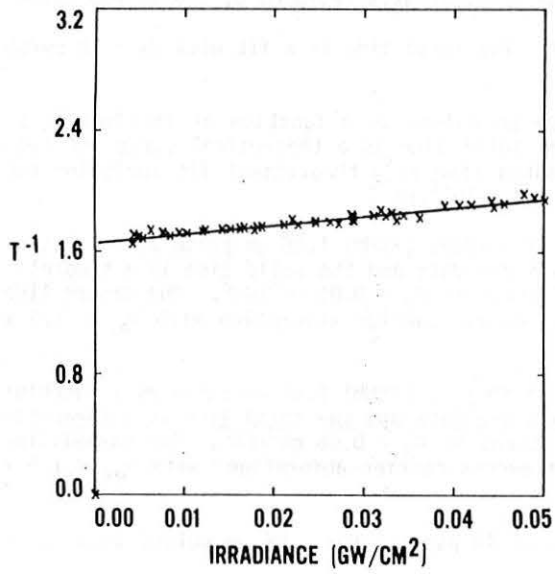


Figure 2

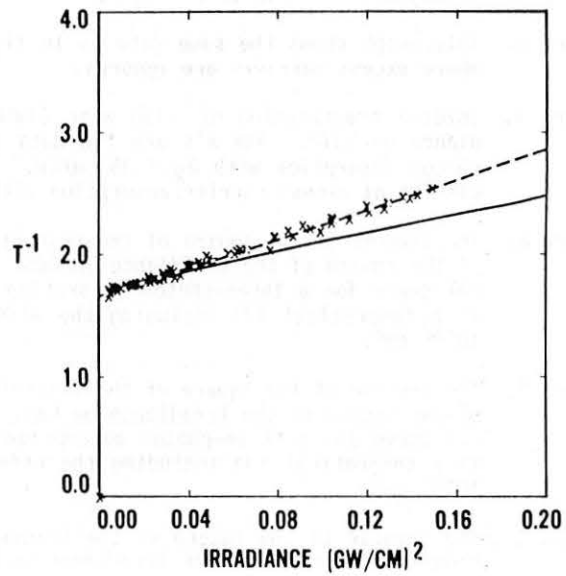


Figure 3

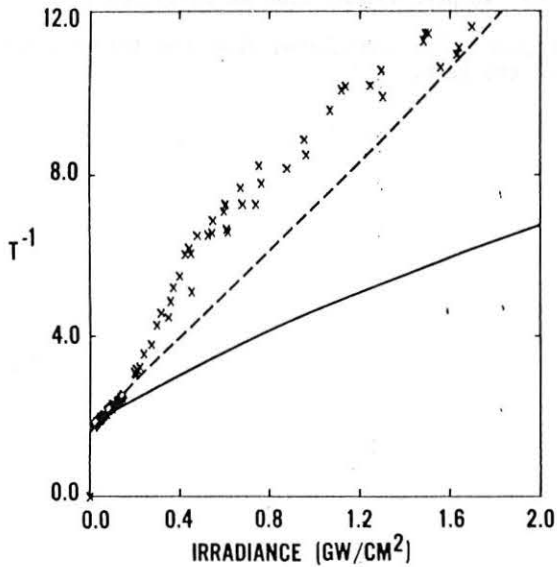


Figure 4

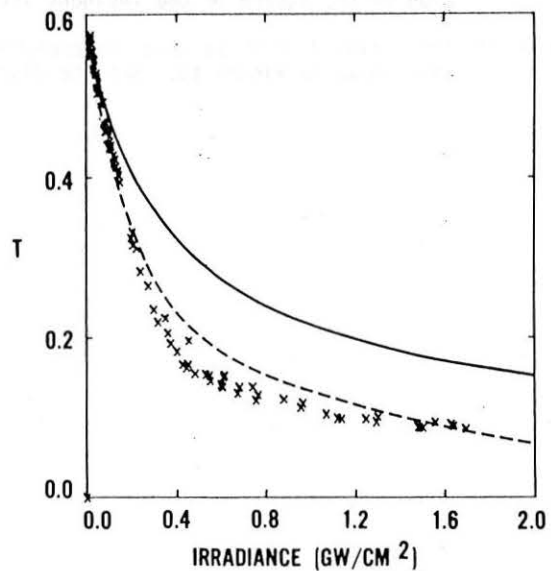


Figure 5

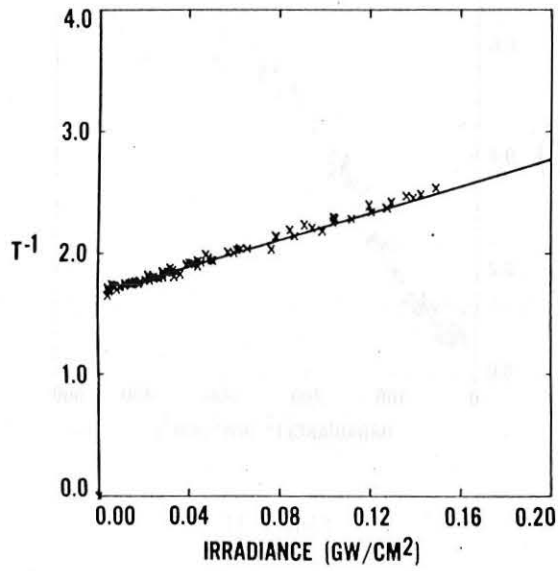


Figure 6

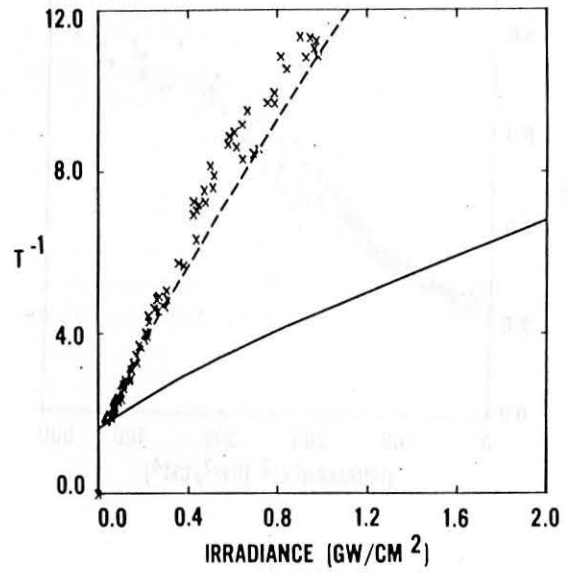


Figure 7

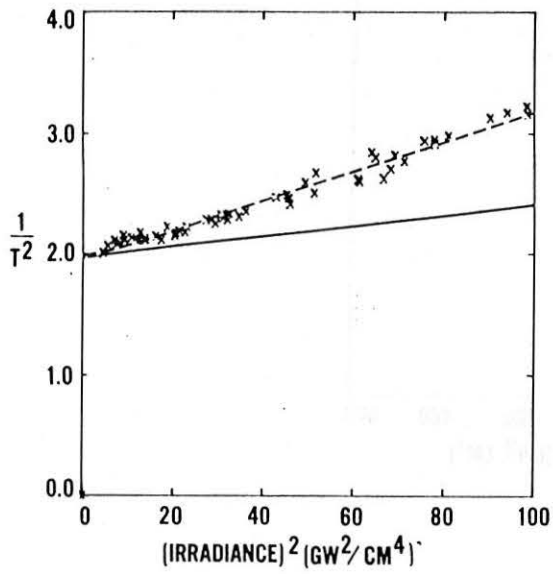


Figure 8

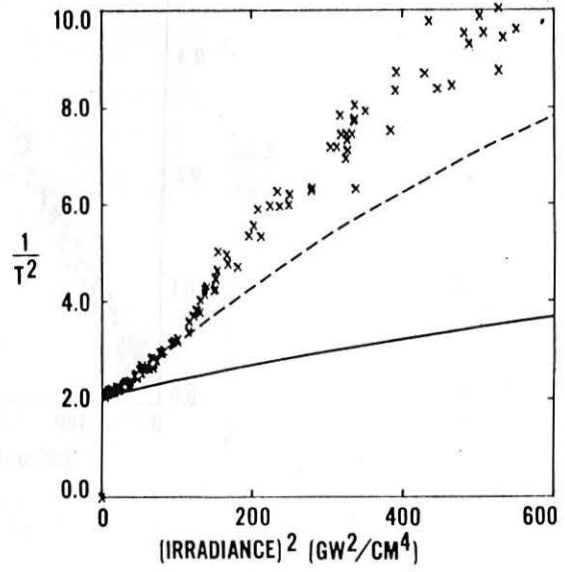


Figure 9

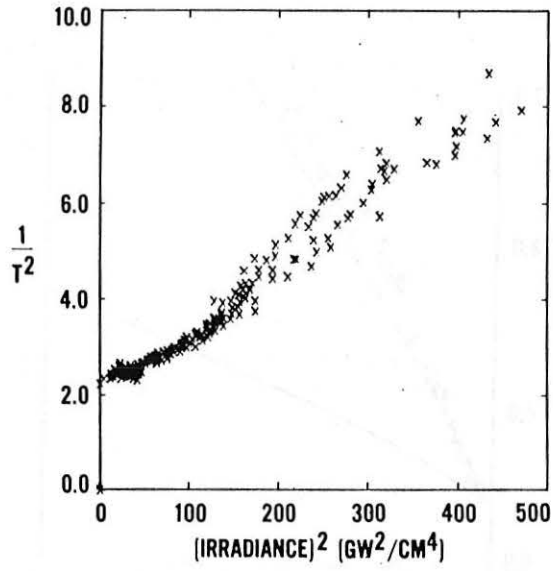


Figure 10

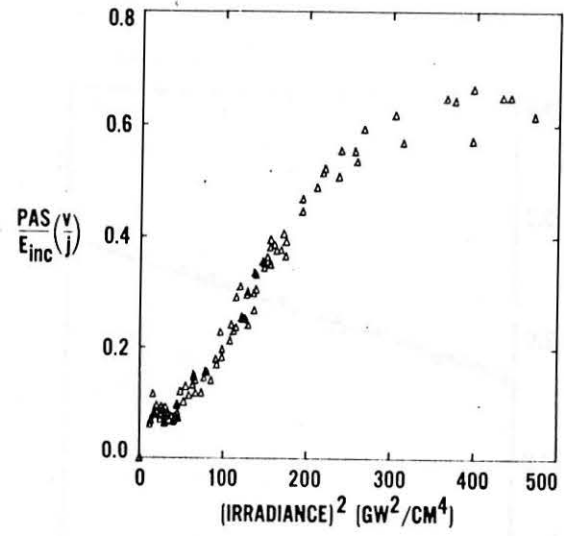


Figure 11

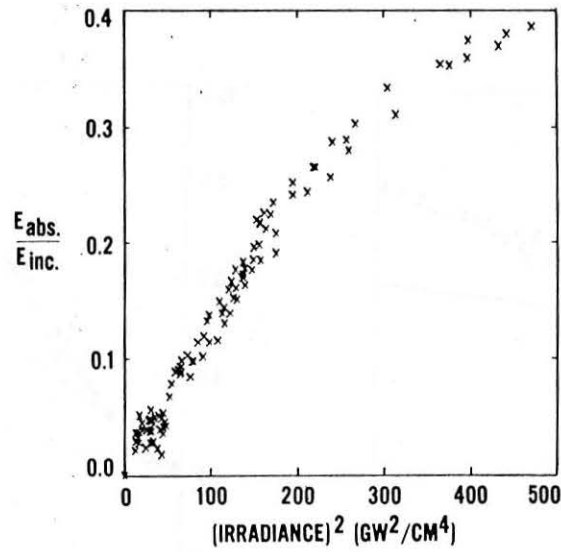


Figure 12